



Cite this: *Nanoscale*, 2015, 7, 218

On stoichiometry and intermixing at the spinel/perovskite interface in $\text{CoFe}_2\text{O}_4/\text{BaTiO}_3$ thin films†

Vasiliki Tileli,^{*a} Martial Duchamp,^b Anna-Karin Axelsson,^{a,c} Matjaz Valant,^{a,d} Rafal E. Dunin-Borkowski^b and Neil McN. Alford^a

The performance of complex oxide heterostructures depends primarily on the interfacial coupling of the two component structures. This interface character inherently varies with the synthesis method and conditions used since even small composition variations can alter the electronic, ferroelectric, or magnetic functional properties of the system. The focus of this article is placed on the interface character of a pulsed laser deposited $\text{CoFe}_2\text{O}_4/\text{BaTiO}_3$ thin film. Using a range of state-of-the-art transmission electron microscopy methodologies, the roles of substrate morphology, interface stoichiometry, and cation intermixing are determined on the atomic level. The results reveal a surprisingly uneven BaTiO_3 substrate surface formed after the film deposition and Fe atom incorporation in the top few monolayers inside the unit cell of the BaTiO_3 crystal. Towards the CoFe_2O_4 side, a disordered region extending several nanometers from the interface was revealed and both Ba and Ti from the substrate were found to diffuse into the spinel layer. The analysis also shows that within this somehow incompatible composite interface, a different phase is formed corresponding to the compound $\text{Ba}_2\text{Fe}_3\text{Ti}_5\text{O}_{15}$, which belongs to the ilmenite crystal structure of FeTiO_3 type. The results suggest a chemical activity between these two oxides, which could lead to the synthesis of complex engineered interfaces.

Received 30th July 2014,
Accepted 3rd November 2014

DOI: 10.1039/c4nr04339a

www.rsc.org/nanoscale

1 Introduction

Advanced heterostructured nanomaterials, such as embedded nanoparticles, heteroepitaxial composite layers, and even bio-hybrids with a functional response, are increasingly investigated for their expanded applications in electronics, materials science, catalysis, energy production, medicine, *etc.* In general, these functional nanostructures respond through a change of a state variable, which may be a change of charge or spin density, a spin or dipole orientation, an excited state, a mechanical deformation, a molecular arrangement, *etc.* In thin film layered composites, the interface becomes as important as the

bulk of the individual layers. Sometimes it can even be considered as a completely new layer as both its physics and its chemistry deviate from either of the two components. The interfacial regions that are commonly found in oxide composites, are often formed from defects, strain, and interdiffusion; sometimes they can be of a completely different crystal structure or chemical composition. When the film thickness goes below about one hundred nanometers, it is very likely that up to about half of the film volume is structurally affected by the interface,¹ which significantly changes its overall properties. In some cases, the new chemistry can be advantageous, like for the $\text{SrTiO}_3\text{-LaAlO}_3$ interface, which the interfacial bonding energies create a highly conductive 2D electron cloud. In some other cases, the interaction between the two layers impedes the desired functional properties, as recently reported for the $\text{LaCrO}_3/\text{SrTiO}_3$ system.²

Spinel and perovskite structures are often combined into a multilayer composite in magnetoelectrics^{3,4} as some of the best magnetostrictive and piezoelectric oxides belong to these crystal groups. For such magneto-electro composites, theoretical models claim that a perfect elastic interface between the magnetostrictive and piezoelectric layers provides optimal magnetoelectric coupling,⁵ assuming that the properties of the parent materials in the composite are not altered during processing. Consequently, any characteristics of the interfaces that will induce structural changes will reduce the magnetoelectric

^aDepartment of Materials, Imperial College London, Exhibition Road, SW7 2AZ London, UK. E-mail: v.tileli@imperial.ac.uk

^bErnst Ruska-Centre for Microscopy and Spectroscopy with Electrons and Peter Grünberg Institute, Forschungszentrum Jülich, 52425 Jülich, Germany

^cSchool of Engineering, London South Bank University, 103 Borough Road, SE1 0AA London, UK

^dMaterials Research Laboratory, University of Nova Gorica, Vipavska 13, Nova Gorica, SI-5000, Slovenia

† Electronic supplementary information (ESI) available: Magnetic moment data of the structure, linear decomposition graph of the interface layer in its constituent components of CoFe_2O_4 and BaTiO_3 , reference Fe $L_{3,2}$ EEL data used for MLLS analysis of the Fe oxidation and coordination variation, and a table detailing the partial ionization cross-sections used for quantitative MLLS analysis. See DOI: 10.1039/c4nr04339a

coupling. This is becoming increasingly important when the layer thickness is limited to nanometer scale. The composite $\text{CoFe}_2\text{O}_4/\text{BaTiO}_3$ system has been studied in many different configurations, such as BaTiO_3 nanopillars vertically clamped to a CoFe_2O_4 matrix,⁶ self-assembled nanostructures,^{7,8} two-phase ceramics,⁹ and planar (*i.e.* layered) heterostructures.¹⁰ It should be pointed out that, despite the vertical nanopillar structure being less clamped to the matrix, conductive interfaces can form and, thus, can electrically shut down the application.¹¹ As a result, much attention is focused on the layered heterostructures where another problem is highlighted. The authors regularly observe a decrease in the magnetization of the CoFe_2O_4 layer after deposition and, consequently, a reduction in magnetoelectric coupling. Although the mechanism of the failure is still not fully understood, it is evident that the problems originate from the interfacial characteristics of the two oxide layers.

To explain the atomistic origin of this problem, it is important to understand what drives the electric and magnetic order in each individual crystal structure. In tetragonal room-temperature BaTiO_3 with a $P4mm$ cell, Ti atoms are displaced along the c -axis and the cell is therefore elongated. This elongation is discrete and its high polar state originates from the mass and charge of the Ba atom. This in turn means that the ferroelectric and piezoelectric properties of BaTiO_3 are very sensitive to the average relative displacement along the polar c -axis cell, which moreover means that impurities and strain would dramatically change these properties. On the other hand, the magnetostrictive oxide, *i.e.* CoFe_2O_4 , has an inverse spinel structure with formula $\text{B}(\text{AB})\text{O}_4$. In an ideal inverse spinel, Co^{2+} ions occupy the octahedral sites and Fe^{3+} ions are equally divided among the remaining octahedral sites and the tetrahedral site. It has a cubic lattice parameter of 8.38 Å, which corresponds to a ~7% lattice mismatch with the (001) BaTiO_3 growth template ($a(\text{CoFe}_2\text{O}_4) = 2a(\text{BaTiO}_3)$). Only an eighth of the tetrahedral sites and half of the octahedral sites are occupied in this spinel. This large fraction of empty interstitial sites creates an open structure that is susceptible to strain effects and readily permits cation migration within the spinel. In reality, the cation occupancy in the CoFe_2O_4 spinel structure deviates from the ideal distribution, which directly affects the magnetic properties due to antiferromagnetic ordering in the two spin sub-lattices.

Typically, the synthesis of spinel-perovskite thin layers proceeds either by pulsed laser deposition (PLD) or by molecular beam epitaxy (MBE). The preferred method is PLD due to its high throughput, ease of use and inexpensive nature compared to MBE. However, control of the composition of heterostructures remains a tantalizing issue for both techniques but, more so, for the highly energetic PLD.² Consequently, the functional properties of complex oxides depend strongly on all processing factors during a typical vacuum film deposition such as atmosphere, pressure, and temperature.

The objective of this paper is to get an insight into the atomic arrangement of the interface of the PLD grown CoFe_2O_4 - BaTiO_3 magnetoelectric thin film system by means of

advanced sub-nanometer transmission electron microscopy techniques. We discuss the role of the BaTiO_3 substrate morphology and polarity on the structural properties of the interface. Furthermore, we report on chemical interdiffusion, cation intermixing, and valence state and coordination instabilities occurring during CoFe_2O_4 film deposition and relate them to the observed deterioration of the magnetoelectric properties. This is the first report to suggest another compound forming at the interface of stoichiometry $\text{Ba}_2\text{Fe}_3\text{Ti}_5\text{O}_{15}$, which is a reduced A-site Ba doped ilmenite of FeTiO_3 type, further corroborating the chemical complexity of the heterostructure.

2 Experimental details

CoFe_2O_4 films were grown by pulsed laser deposition (PLD) at 550 °C on (001) BaTiO_3 single crystal substrate. Details of the deposition have been reported elsewhere.¹² Film thicknesses ranged from 13–100 nm. All films show similar interfacial characteristics and, for the work here, the sample of 75 nm thick film was analyzed. Cross-sectional specimens were prepared by focused ion beam milling and final thinning was performed with low energy Ar ions (0.5 eV) using a Fischione NanoMill system. Structural investigations were performed using an FEI Titan transmission electron microscope (TEM) equipped with a spherical aberration corrector at the image plane (London, UK). For all TEM micrographs, the corrector was tuned to $-13 \mu\text{m}$. High angle annular dark field (HAADF) scanning transmission electron micrographs (STEM) and chemical investigations were carried out using an FEI Titan double corrected TEM equipped with a Gatan Quantum electron energy-loss (EEL) spectrometer (Jülich, Germany) with an electron energy of 200 keV. The STEM resolution was of 0.8 Å. Electron energy-loss spectroscopy (EELS) data were acquired with an energy resolution of 700 meV and an energy dispersion of 0.2 eV per channel. The spectrum image (SI) analysed here was 182×22 pixels and it was acquired with 0.51 Å step size. It is noted that multiple EEL SIs were acquired and no significant compositional variations were detected across the interface. The EEL spectrum image analyzed below was acquired at a collection semi-angle of 40 mrad and a convergence semi-angle of 20 mrad. To reduce noise in the HAADF STEM images from Fig. 1(d) and Fig. 5(a) below, a gaussian low pass filter of 0.015 nm σ was applied. Simulations of atomic positions were performed using Vesta software¹³ and STEM images were calculated using Dr Probe software.¹⁴ Finally, we note that the projected final cross-section thickness of the specimen analysed was ~10 nm for the TEM measurements and on the order of 50 nm for the STEM/EELS analysis.

3 Results and discussion

The local structure of the system $\text{CoFe}_2\text{O}_4/\text{BaTiO}_3$ was evaluated by TEM, as shown in Fig. 1(a–c), and by STEM, as shown

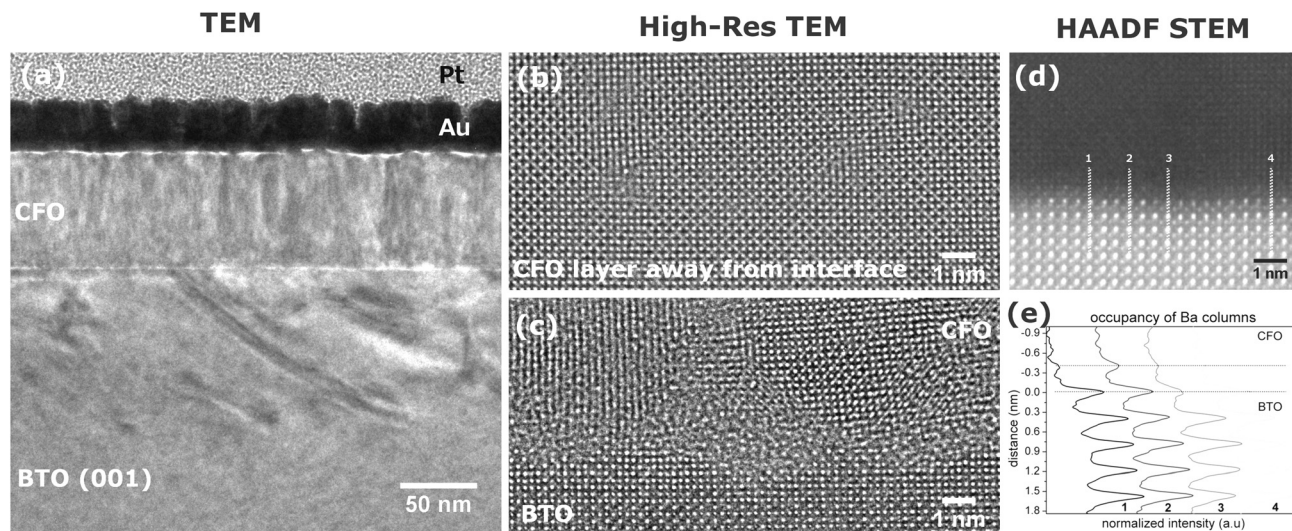


Fig. 1 (a–c) TEM and (d) STEM micrographs of the local structure in the CoFe_2O_4 (CFO) film on BaTiO_3 (BTO). The low magnification image (a) demonstrates the strained substrate surface propagating for 100 nm into the bulk. The disorder at the interface (c) results in dislocations and defects well into the CFO layer (b). The HAADF-STEM image (d) reveals an imperfect substrate surface and (e) demonstrates the variation of the Ba atom occupancy vertically across the interface (projected as zero distance) in the four numbered regions shown in (d).

in Fig. 1(d and e). The impact of the growth of the film on the highly polar BaTiO_3 substrate is demonstrated well in Fig. 1(a) where contrast variations due to strain effects are extended over 100 nm into the substrate. The film is epitaxially grown (also revealed by XRD¹) and it proceeds with a columnar character. The strain induced by the 7% lattice mismatch is compensated by minor rotations of unit cells and dislocations. A low density of dislocations is integrated throughout the CoFe_2O_4 film, as shown in Fig. 1(b). High-resolution (High-Res) TEM is sensitive to the phase of the exit surface electron wave. In this case (Fig. 1(c)), the interface appears as a low crystallinity layer with a varying thickness profile. This highly defective interface is adopted to compensate for the enhanced strain of the surface layer induced by the intrinsic strong surface polarization fields, as previously argued.¹⁵ In addition, BaTiO_3 develops a surface step structure during film deposition. Evidence of atomic intermixing in the last 3 unit cells of the substrate can be seen on the left side of the Fig. 1(d). These issues are expected to further introduce hindrances on the film growth. STEM is more sensitive to the atomic number of the chemical element present in the structure and, under the HAADF imaging mode, diffraction and strain effects are minimized. In the HAADF STEM image of the interface (Fig. 1(d)), the role of the imperfect substrate surface is augmented. For a qualitative evaluation of the occupancy of Ba columns near the interface, histograms taken from across the interface are plotted in Fig. 1(e). The comparison indicates atomically imperfect interfacial planes at the substrate surface where the occupancy of Ba varies significantly along the same unit cell and, in cases, it is half the value of the bulk. Such disorder of the surface structure of the substrate suggests a variation of the bound surface charge density that is responsible for the ferroelectric polarization and, thus, it reflects the quality of the magnetoelectric coupling of the composite.

The local structural environment is related to the stoichiometry and the chemistry at the interface by quantitative analysis of core-loss EEL spectra. Fig. 2 shows typical atomically-resolved EEL spectra and a corresponding annular dark field (ADF) STEM image extending from the pure perovskite substrate into the fully spinel film. The raw EEL spectra demonstrate high mobility of Fe, Ba, and Ti across the interface. Fe seems to be incorporated into the BaTiO_3 unit cells near the interface. According to previous studies in ceramics,¹⁶ Fe can substitute both A and B sites in BaTiO_3 and, in both cases, the end result is a decrease of the ferroelectric polarization of the perovskite. Accordingly, in the case of this thin film structure, the interfacial strain can induce further decrease of the surface polarization. In the CoFe_2O_4 film, the EEL spectra indicate Ba and Ti diffusion by ~ 3 nm from the interface. Substitution of diamagnetic ions (Ba, Ti) for paramagnetic ions (Co, Fe) in the spinel can reduce the magnetization and Néel temperature and eventually lead to a paramagnetic room-temperature system.

The transition between the two structures can be effectively monitored by following the oxygen K edge, which is shown alongside all major peaks in Fig. 2(a). The O K fine structure in the substrate, which is shown in the lowest spectrum and it is better monitored in Fig. 3(b), contains four characteristic peaks (a–d) reflecting the perovskite lattice.^{17–19} In detail, the first peak (a) is related to the hybridization of the titanium 3d orbitals and the oxygen 2p orbitals, the second peak (b) is dominated by Ba–O interactions, whereas the third (c) and fourth (d) peaks arise from scattering at the nearest oxygen shell.²⁰ On the other side of the interface, in the upper spectrum, the O energy-loss near edge fine structure (ELNES) for CoFe_2O_4 shows inverse spinel characteristics in accordance with previous studies.^{21,22} In particular, transitions to states created by the hybridisation of oxygen 2p take place with three

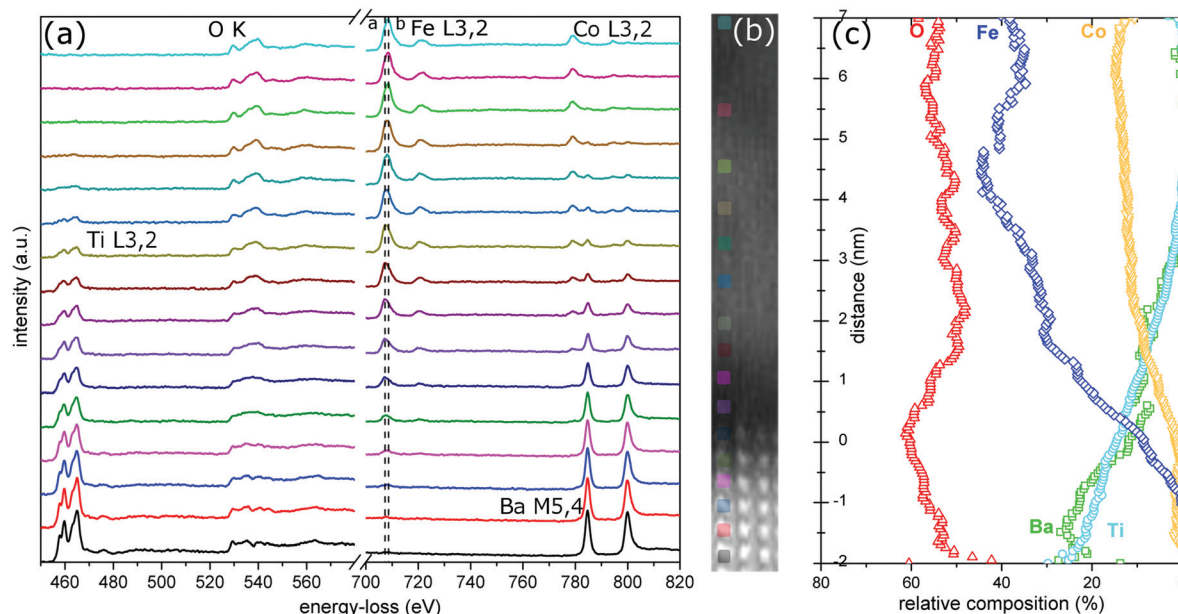


Fig. 2 (a) EEL spectra showing the Ti L_{3,2}, O K, Fe L_{3,2}, Co L_{3,2}, and Ba M_{5,4} edges and (b) a corresponding annular dark field (ADF) image showing the evolution of the thin film structure. The beginning of the interface is defined at 0 (nm). (c) Calculated relative compositional profiles for all elements in the system indicating the extensive, disparate character of the interface.

types of 3d orbitals; the first peak (a) is attributed to a tetrahedrally co-ordinated iron(III) orbital, whereas the broad peak (b) arises due to octahedrally co-ordinated orbitals for both iron(III) and cobalt(II) ions.

The interface between the two structures extends over several nanometers and the chemical transition, inferred from the EEL spectra, is much wider than the dark interfacial contrast visible in STEM images, and it is not confined to a monolayer as reported for the BaTiO₃/Fe system recently.²³ The O K edge fine structure becomes broad at position 0 (reflecting the beginning of the interface), when a significant amount of Fe is incorporated into the BaTiO₃ unit cell. Multiple linear least squares (MLLS) analysis of the interface O K edge with spectra from the outer “bulk-like” BaTiO₃ and CoFe₂O₄ fine structures suggests that the interface is not composed of the two distinct structures but consists of a different phase (see Fig. S2†). In order to obtain information about this interfacial phase, quantification of the EEL spectra was performed. The relative composition of the different elements was established by carrying out quantitative analysis by integrating the intensities of the ionization edges related to the partial ionization cross-sections.²⁴ For example, for the Ba M edge and the Ti L edge the ratio of the absolute numbers *N* of atoms per unit area in the specimen can be expressed in the form:

$$\frac{N_{\text{Ba}}}{N_{\text{Ti}}} = \frac{I_{\text{M}}^{\text{Ba}} \sigma_{\text{L}}^{\text{Ti}}}{I_{\text{L}}^{\text{Ti}} \sigma_{\text{M}}^{\text{Ba}}} \quad (1)$$

Values of the ionization cross-sections (σ) of Ba M, Ti L, Fe L, and Co L edges were calculated using (i) standard spectra taken from bulk BaTiO₃ and “bulk-like” CoFe₂O₄ taken several nanometers away from interface and (ii) the calculated O K

edge cross-section using Hartree–Slater methods implemented in DigitalMicrograph software (assumed to be a good approximation for K edges of light elements). These corrected ionization cross-sections were used to quantify the amount of each element and plot the calculated quantification profiles *versus* depth, which are shown in Fig. 2(c). The calculated cross-sections and the integration ranges are shown in Table S1.† The average error in the analysis is estimated to ~10%, which includes contributions from the background subtraction, integration window widths, and cross-section calculations.²⁴

At the interface (position 0 at Fig. 2(c)) the relative extracted composition corresponds to a compound of stoichiometry Ba₂Fe₃Ti₅O₁₅. This compound can be reduced to the ilmenite structure assuming that Ba²⁺ ions occupy a proportion of the Fe sites, which should be of 2+ valency to ensure charge neutrality. Indeed, the shift of the Fe L₃ edge at the interface towards lower energy losses is already visible in the raw spectra (Fig. 2(a)). Ilmenite-derived materials have been reported to show A-site-driven geometric ferroelectricity.²⁵ Two nanometers away from the interface, at position 2, the quantitative analysis suggests a structure of BaTiCo₂Fe₄O₁₀. The spectra shown in Fig. 3 suggest incorporation of Ba²⁺ ions on the Co sites and Ti⁴⁺ ions on the Fe sites. Both valence states of iron are found. When Ti is incorporated into the lattice, the Fe oxidation state is reduced. The O K edge indicates a spinel-like character of the structure, with distinct a and b peaks. It is noted that inspection of the Ti L₃ edge shows similar features across the interface, with no indication of a possible reduction of the valence state of Ti from 4+ to the magnetic 3+ state (although its determination from EELS results is challenging depending on the relative proportion of the two oxidation states).

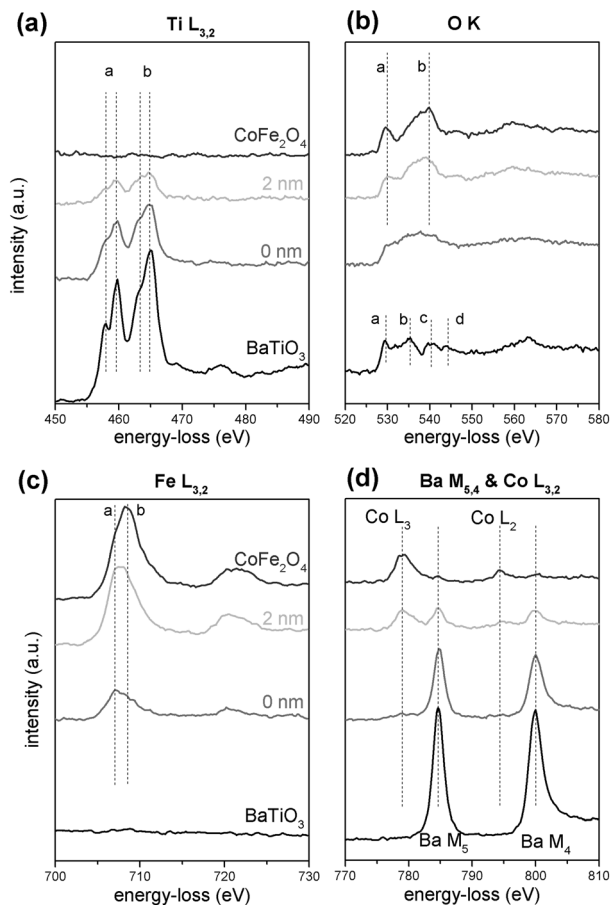


Fig. 3 ELNES for the core loss edges of (a) Ti $L_{3,2}$, (b) O K, (c) Fe $L_{3,2}$ and (d) Ba $M_{5,4}$ and Co $L_{3,2}$ showing the evolution of the structure from BaTiO₃ towards the interface at position 0 (nm), at position 2 (nm), and within the fully inverse CoFe₂O₄ spinel film. For the positions of the distances along the interface, refer to the HAADF image of Fig. 2(b). The characteristic peak positions for each ion are indicated for clarity.

To evaluate the predicted structures, Fe valence maps were calculated using a multiple linear least squares algorithm in DigitalMicrograph software. Standard spectra (shown in Fig. S3†) were used for octahedrally coordinated O_h Fe²⁺ (ref 26) and for tetrahedrally T_d and octahedrally coordinated O_h Fe³⁺ (ref. 27). The profiles of the fitted coefficients for each valence and coordination state of Fe and the corresponding maps are shown in Fig. 4. The O_h Fe²⁺ signal dominates the interface, it peaks at position 2 nm and then it linearly decreases further away from the interface. CoFe₂O₄ standard spectra taken 17 nm from the interface show a diminishing amount of 2+ oxidation state of Fe. The change of the coordination of the Fe 3+ oxidation state is related to the evolution towards the fully spinel structure. The interface, position 0, is dominated by Fe 2+ oxidation state and any spinel inversion measurement is not possible. However, already from Fig. 4, the ratio $Fe_{O_h^{3+}} : Fe_{T_d^{3+}}$ at position 7 (nm) is seen to be equal to 2:1, corresponding to a fully inverse spinel structure. It is noted that the degree of inversion of the spinel CoFe₂O₄ has been related to the magnetic moment previously both

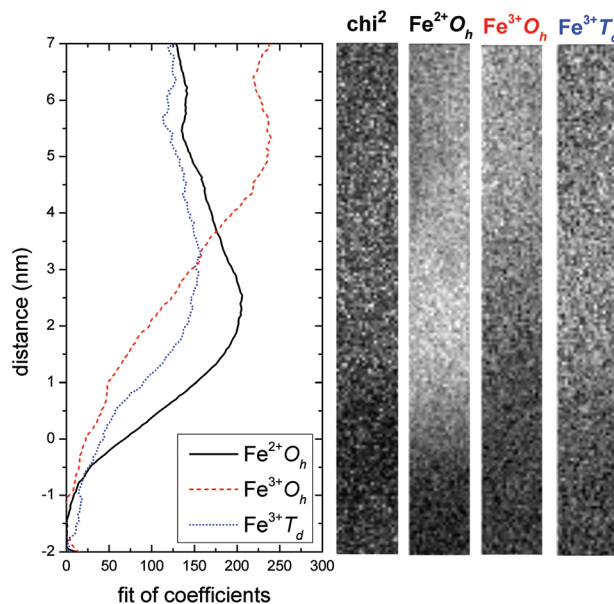


Fig. 4 Multiple linear least squares (MLLS) fit of coefficients along the spectrum image in Fig. 2. The fit was computed using standard spectra for the octahedrally O_h coordinated Fe²⁺ and the tetrahedrally T_d and octahedrally O_h coordinated Fe³⁺. The maps of each of the components indicate a high concentration of the 2+ oxidation state of Fe at the interface.

experimentally²⁸ and theoretically.²⁹ All previous studies suggest that the total magnetic moment decreases with decreasing inversion, inducing an exchange mechanism of Co ions on octahedral sites with tetrahedrally coordinated Fe ions. Therefore, the reduced magnetic moment in such thin films (Fig. S1†) is attributed to the fact that a significant part of the film right at the interface is not fully inverted.

In an attempt to relate the chemical results to the structural character of the CoFe₂O₄–BaTiO₃ interface, a predicted model structure of a perfect interface is super-imposed on a representative HAADF STEM image, seen in Fig. 5(a). For the atomic layer stacking at the interface, a terminating layer of TiO₂ was considered on the substrate and an Fe–O terminating layer on the CoFe₂O₄ (001), which reflects the Fe-rich interface, as deduced from the EELS results. This model is clearly not plausible since the regular spinel structure is not in contact with the substrate surface. Based on the chemical analysis, for the intermediate layer (about 2 nm thick), we consider a super-cell along

$$\begin{pmatrix} 1 & -1 & 0 \\ 1 & 1 & 0 \\ 0 & 0 & 1 \end{pmatrix}$$

of the trigonal $R3c$ ilmenite structure. This supercell configuration ($a = 0.89$ nm) is chosen to match the growth lattice parameter of the perovskite ($2a = \sim 0.8$ nm) and spinel ($a = 0.838$ nm) structures, as shown in Fig. 5(c). The atomically predicted image simulation fails to reproduce the experimental HAADF image, since the materials are a poor match along the b axis with the ilmenite's primitive cell being 14 nm wide. The

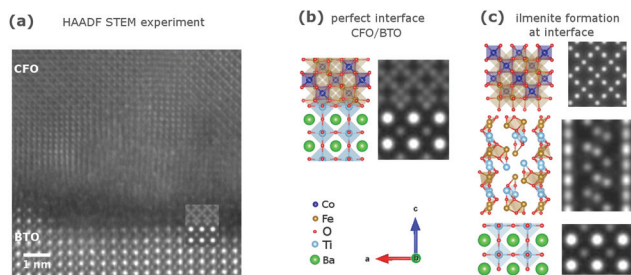


Fig. 5 (a) HAADF STEM image of the interface between CoFe₂O₄ and BaTiO₃ with a superposition of the simulated, perfect interface positioned at the terminating BaTiO₃ layer. The atomic model and HAADF image simulation of the perfect interface are shown in (b). (c) Shows the atomic model and corresponding image simulations of the combined result, inclusive of the intermediate ilmenite supercell.

interfacial atomic disorder seen in the experimental results is a reflection of the *b* axis mismatch. In addition, chemical intermixing further promotes the disorder. It is noted that such an ilmenite structure is a confirmed multiferroic material³⁰ that shows significant promise for strong coupling of the electric and magnetic moments. In this case, however, the introduction of such an interfacial layer effectively inhibits the elastic interaction of the separate magnetoelectric components and thus reduces the magnetic moment of the spinel thin film, as previously published.¹

4 Conclusions

Our findings reveal for the first time on an atom-by-atom scale the chemical complexity of the heteroepitaxy between CoFe₂O₄ and BaTiO₃ along the (001) crystallographic direction. The inherent polarity of the substrate results in surface strain at both sides of the interface. This strain propagates for about 100 nm into the bulk substrate whereas at the CoFe₂O₄ side it is accommodated by defects and dislocations. The adopted, highly disordered interfacial structure is ~2 nm thick and it is non-stoichiometric. In addition, the Fe is reduced to the 2+ oxidation state and the spinel full inverses only after ~5 nm into the film. Quantitative analysis uncovered an ilmenite-like structure as the immediate interfacial layer. The results provide structural and chemical evidence of the incompatibility of the ferroelectric BaTiO₃ with the ferrimagnetic CoFe₂O₄. Ultimately, the failure to control the quality at the interface impedes the elastic strain effects required for the strong magnetoelectric coupling of the composite system. It is noted that although the above results were acquired from a thin film grown under specific conditions, it is expected that, at some degree, the stoichiometry and intermixing of the two oxides will prevail for highly energetic techniques such as pulsed laser deposition.

Acknowledgements

The authors are grateful to Dr Giuseppe Mallia for fruitful discussions concerning the atomic modeling of the interface. The

research leading to these results has received funding from the People Programme (Marie Curie Actions) of the European Union's Seventh Framework Programme (FP7/2007-2013) under REA grant agreement no [301838]. The authors acknowledge further financial support from the EU under the Seventh Framework Programme under grant Agreement 312483-ESTEEM2 (Integrated Infrastructure Initiative I3).

References

- 1 A.-K. Axelsson, F. Aguesse, V. Tileli, M. Valant and N. M. Alford, *J. Alloys Compoud.*, 2013, **578**, 286–291.
- 2 L. Qiao, K. H. L. Zhang, M. E. Bowden, T. Varga, V. Shutthanandan, R. Colby, Y. Du, B. Kabius, P. V. Sushko, M. D. Biegalski and S. A. Chambers, *Adv. Funct. Mater.*, 2013, **23**, 2953–2963.
- 3 M. Fiebig, *J. Phys. D: Appl. Phys.*, 2005, **38**, R123–R152.
- 4 W. Eerenstein, N. D. Mathur and J. F. Scott, *Nature*, 2006, **442**, 759–765.
- 5 M. I. Bichurin, V. M. Petrov and G. Srinivasan, *J. Appl. Phys.*, 2002, **92**, 7681–7683.
- 6 H. Zheng, J. Wang, S. E. Lofland, Z. Ma, L. Mohaddes-Ardabili, T. Zhao, L. Salamanca-Riba, S. R. Shinde, S. B. Ogale, F. Bai, D. Viehland, Y. Jia, D. G. Schlom, M. Wuttig, A. Roytburd and R. Ramesh, *Science*, 2004, **303**, 661–663.
- 7 H. Zheng, J. Wang, L. Mohaddes-Ardabili, M. Wuttig, L. Salamanca-Riba, D. G. Schlom and R. Ramesh, *Appl. Phys. Lett.*, 2004, **85**, 2035–2037.
- 8 D. H. Kim, N. M. Aimon, X. Sun and C. A. Ross, *Adv. Funct. Mater.*, 2014, **24**, 2334–2342.
- 9 J. Van Den Boomgaard, A. M. J. G. Van Run and J. V. Suchtelen, *Ferroelectrics*, 1976, **10**, 295–298.
- 10 R. V. Chopdekar and Y. Suzuki, *Appl. Phys. Lett.*, 2006, **89**, 182506.
- 11 Y.-H. Hsieh, J.-M. Liou, B.-C. Huang, C.-W. Liang, Q. He, Q. Zhan, Y.-P. Chiu, Y.-C. Chen and Y.-H. Chu, *Adv. Mater.*, 2012, **24**, 4564–4568.
- 12 F. Aguesse, A.-K. Axelsson, M. Valant and N. M. Alford, *Scr. Mater.*, 2012, **67**, 249–252.
- 13 K. Momma and F. Izumi, *J. Appl. Crystallogr.*, 2008, **41**, 653–658.
- 14 J. Barthel and L. Houben, *Dr. Probe, High-resolution (S)TEM image simulation software*, 2013, <http://www.er-c.org/barthel/drprobe/index.html>.
- 15 F. L. English, *J. Appl. Phys.*, 1968, **39**, 3231–3236.
- 16 N. Maikhuri, A. K. Panwar and A. K. Jha, *J. Appl. Phys.*, 2013, **113**, 17D915.
- 17 N. Browning, D. Wallis, P. Nellist and S. Pennycook, *Micron*, 1997, **28**, 333–348.
- 18 F. M. F. de Groot, M. Grioni, J. C. Fuggle, J. Ghijsen, G. A. Sawatzky and H. Petersen, *Phys. Rev. B: Condens. Matter*, 1989, **40**, 5715–5723.
- 19 M. Bugnet, G. Radtke and G. A. Botton, *Phys. Rev. B: Condens. Matter*, 2013, **88**, 201107.

- 20 J. Zhang, A. Visinoiu, F. Heyroth, F. Syrowatka, M. Alexe, D. Hesse and H. S. Leipner, *Phys. Rev. B: Condens. Matter*, 2005, **71**, 064108.
- 21 W. F. Pong, M. H. Su, M.-H. Tsai, H. H. Hsieh, J. Y. Pieh, Y. K. Chang, K. C. Kuo, P. K. Tseng, J. F. Lee, S. C. Chung, C. I. Chen, K. L. Tsang and C. T. Chen, *Phys. Rev. B: Condens. Matter*, 1996, **54**, 16641–16645.
- 22 S. Gautam, S. Muthurani, M. Balaji, P. Thakur, D. P. Padiyan, K. H. Chae, S. S. Kim and K. Asokan, *J. Nanosci. Nanotechnol.*, 2011, **11**, 386–390.
- 23 L. Bocher, A. Gloter, A. Crassous, V. Garcia, K. March, A. Zobelli, S. Valencia, S. Enouz-Vedrenne, X. Moya, N. D. Marthur, C. Deranlot, S. Fusil, K. Bouzehouane, M. Bibes, A. Barthelemy, C. Colliex and O. Stephan, *Nano Lett.*, 2012, **12**, 376–382.
- 24 R. F. Egerton, *Electron energy-loss spectroscopy in the electron microscope*, Plenum Press, New York, NY, 1986.
- 25 N. A. Benedek and C. J. Fennie, *J. Phys. Chem. C*, 2013, **117**, 13339–13349.
- 26 G. Radtke, S. Lazar and G. A. Botton, *Phys. Rev. B: Condens. Matter*, 2006, **74**, 155117.
- 27 S. Turner, J. Verbeeck, F. Ramezanipour, J. E. Greedan, G. Van Tendeloo and G. A. Botton, *Chem. Mater.*, 2012, **24**, 1904–1909.
- 28 G. A. Sawatzky, F. VAN DER Woude and A. H. Morrish, *J. Appl. Phys.*, 1968, **39**, 1204–1205.
- 29 Y. H. Hou, Y. J. Zhao, Z. W. Liu, H. Y. Yu, X. C. Zhong, W. Q. Qiu, D. C. Zeng and L. S. Wen, *J. Phys. D: Appl. Phys.*, 2010, **43**, 445003.
- 30 T. Varga, A. Kumar, E. Vlahos, S. Denev, M. Park, S. Hong, T. Sanehira, Y. Wang, C. J. Fennie, S. K. Streiffer, X. Ke, P. Schiffer, V. Gopalan and J. F. Mitchell, *Phys. Rev. Lett.*, 2009, **103**, 047601.